Estimating internal wave spectra using constrained models of the dynamic ocean

E. Vsemirnova,[1] R. Hobbs,[1] N. Serra,[2] D. Klaeschen,[3] and E. Quentel[4]

Received 15 June 2009; revised 9 September 2009; accepted 30 September 2009; published 31 October 2009.

[1] Multi-Channel Seismic method (MCS), with its ability to image events down to a lateral resolution of 10 m has been successfully applied to address questions in physical oceanography. However, to date, these analyses have overlooked an important detail; the imaged boundaries are dynamic and move on a timescale that can be resolved by the MCS method. An important step in understanding the effect of the movement is calibration against constrained models. We demonstrate in this paper that it is possible using careful interpolation to take high resolution models of dynamic water (160 m $\times$ 2 m spatial resolution and 15 min temporal resolution) and generate models for synthetic seismic simulations (20 m $\times$ 4 m spatial resolution and 20 sec temporal resolution). We show that moving water, when ignored, will distort analyses of wavenumber spectra estimated from seismic data since the relative movement of water masses and the seismic acquisition vessel will change the apparent slope of spectra. **Citation:** Vsemirnova, E., R. Hobbs, N. Serra, D. Klaeschen, and E. Quentel (2009), Estimating internal wave spectra using constrained models of the dynamic ocean, *Geophys. Res. Lett.*, *36*, L00D07, doi:10.1029/2009GL039598.

1. Introduction

[2] Recent research [*Holbrook et al.*, 2003] has shown that MCS, developed by hydrocarbon industry to provide detailed images of the sub-surface, can be used to image boundaries in the oceans. The horizontal resolution of the images is about 10 m, which is over two orders of magnitude better than the resolution of typical oceanographic surveys.

[3] One of the objectives of the interdisciplinary GO (Geophysical Oceanography) project is to provide the necessary benchmark calibration between reflection seismic and oceanographic data sets [*Hobbs*, 2007]. The selected target area is the Mediterranean water outflow through the Strait of Gibraltar into the Gulf of Cadiz. This region has extensive databases for both seismic and oceanographic data, a variety of oceanographic features including margin slope, rough sea-bed topography and large eddy currents (Meddies); and the strong oceanographic signature of Mediterranean water [*Ambar et al.*, 2002]. A combined dataset with simultaneous and co-located seismic and oceanographic data was successfully acquired, but raised the question of what, if any, are the effects of relative movement of water and vessel during acquisition. Direct evidence was observed on two profiles shot in opposite directions (Figure 1). These show an asymmetry in the apparent structures.

[4] To resolve these issues, to understand how the water layer reflectvity is created and how it is affected by movement, we computed a high quality synthetic seismic dataset over a dynamic model of the ocean. A major issue was reconciling the length and time scales used for ocean modelling with the requirements for seismic wavefield simulations.

2. Modelling Set-up

[5] An underlying assumption of the seismic reflection method is that the subsurface boundary is fixed both in time and space. This is not true for boundaries in water. These are dynamic and the larger-amplitude lower-frequency internal waves, which are the easiest to map, are those moving with the fastest velocity, which maybe on the order of one meter per second. This speed is significant when compared to the velocity of the seismic acquisition vessel, which is typically 2 to 3 m/s.

[6] To test this effect, we use a simple model – an internal wave surface given by cosine function with a wavelength of 2 km and an amplitude of 20 m. The code we used for our seismic simulation is a modified phase-screen code [*Wild et al.*, 2000]. Figure 2 shows stacked sections for 2D synthetics for the seismic survey over 3 targets:

[7] 1. Static case, vessel is moving across the profile, but boundary is static (v_{ship} = 2 m/s).

[8] 2. Vessel and boundary are moving in the same direction (v_{ship} = 2 m/s, v_{water} = 1 m/s).

[9] 3. Vessel and boundary are moving in opposite directions (v_{ship} = 2 m/s, v_{water} = -1 m/s).

[10] Acquisition receiver parameters are similar to those used on the GO experiment: 192 channel receiver array with 6.25 m spacing between receivers [*Hobbs*, 2007]; shot spacing 10 sec/20 m.

[11] The apparent wavelength of the wave seen on each image, follows by the relationship $\lambda_{mod} = v_{ship}\lambda_{true}/(v_{ship} - v_{water})$. In case (1) we see the true wavelength of 2 km, however in case (2) it appears with a wavelength of 4 km and case (3) it appears with wavelength of 1.333 km.

[12] This example shows that the results we obtained above the moving simple target using the seismic reflection method are distorted. The conclusion is that when using images from (2) or (3) "as they are" to map spectra the wavenumber will be shifted. Extending this simple analysis predicts that relative movement of the target with respect to

[1]Earth Sciences Department, Durham University, Durham, UK.
[2]Institute of Oceanography, Hamburg University, Hamburg, Germany.
[3]Leibniz Institute of Marine Sciences at Kiel University (IFM-GEOMAR), Kiel, Germany.
[4]LDO, UMR 6538, IUEM, Brest University, CNRS, Plouzane, France.

0094-8276/09/2009GL039598$05.00

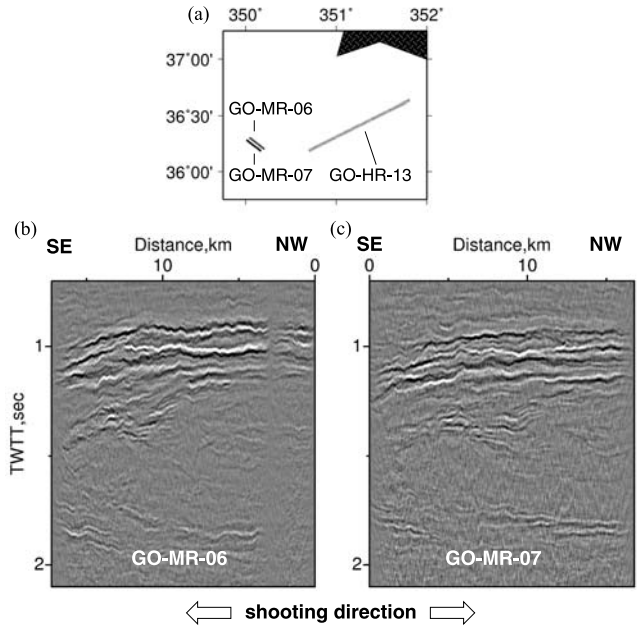

Figure 1. (a) Locations of seismic profiles from the GO experiment: GO-MR-06, GO-MR-07 and GO-HR-013. MR denotes "medium resolution" frequency band and "HR" denotes for high resolution band [*Hobbs*, 2007]. (b) Part of seismic profile GO-MR-06; (c) part of seismic profile GO-MR-07. The same reflector groups can be recognised on both images, but the reflector undulations look more flat for GO-MR-07.

the vessel will change the apparent slope of wavelength spectra estimated from seismic data. By correcting the geometry of the relative movement of ship and water the correct wavelength can be recovered, but then we face another question of how to correct for unknown movement. In real data this is probably spatial and depth dependent.

3. Available Oceanographic Models

[13] In order to develop and demonstrate our analysis we applied the same approach to a more sophisticated oceanographic model. We used the "Regional Ocean Modelling System" – ROMS [*Haidvogel et al.*, 2000], a primitive equations numerical ocean model, configured as a rotating "dam break" experiment. *Serra et al.* [2005] demonstrated that this code was suitable to model the complex interactions in the Gulf of Cadiz in 3D. However the synthetic oceanographic 2D dataset presented here was specifically designed to model mesoscale structures without recourse to computationally expensive 3D simulations.

[14] The setting mimics the overflow of Mediterranean Water from the Alboran Sea into the Gulf of Cadiz across the Strait of Gibraltar and the penetration of the plume in the Gulf of Cadiz. Associated fundamental large-scale mixing and entrainment processes are preserved and contribute to the realism and relevance of the simulations. In this model the dense water spills from the reservoir basin into the receiving stratified environment. Above the dense water, fresher and lighter water counter-flows into the reservoir, establishing a 2-layer system (Figure 3a), which is a well-known feature in the Strait of Gibraltar [*Armi and Farmer*, 1988].

[15] The idealized configuration presents, nonetheless, some limitations concerning the representation of specific mixing processes occurring in the dense plume. The parameterization of mixing processes (which are definitely not resolved even with a 160 m resolution) is always troublesome since there are not systematic observations of these small-scale processes. However, from the large-scale evolution of the flow, namely its entrainment rate, rate of descent and level of neutral buoyancy, one can assume that the parameterization is accounting for the unresolved processes. Figure 3b represents a temperature section co-located with GO-HR-13 seismic (see location of the profile in Figure 1a).

[16] The initial oceanographic model does not include sharp contrasts between the different water masses, so the reflectivity is frequency dependent [*Ruddick et al.*, 2009]. Hence we compute our synthetic using a Ricker wavelet with a peak frequency of 10 Hz because for this model only frequencies below 20 Hz are reflecting from the water mass boundaries.

[17] In the study we use the phase screen code [*Wild et al.*, 2000] which is robust against numerical dispersion that limits the use of FD based codes [*Kelly et al.*, 1976], but which suffers from wrap-around because it models wave propagation in Fourier space. We can reliably model our 10 Hz Ricker wavelet on a 20 m grid. However to match

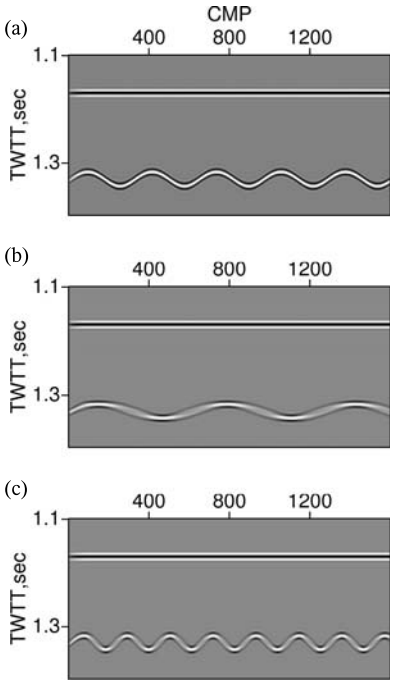

Figure 2. Stack for 2D synthetics over 3 targets: (a) static case, vessel is moving across the profile, but the boundary is static; (b) vessel and boundary are moving in the same direction; (c) vessel and boundary are moving in opposite directions. An internal wave surface is given by a cosine function with wavelength 2 km and amplitude of 20 m. The flat reflector on the top is a reference boundary. The apparent wavelength is 4 km for Figure 2b and 1.333 km for Figure 2c compared to the true wavelength of 2 km.

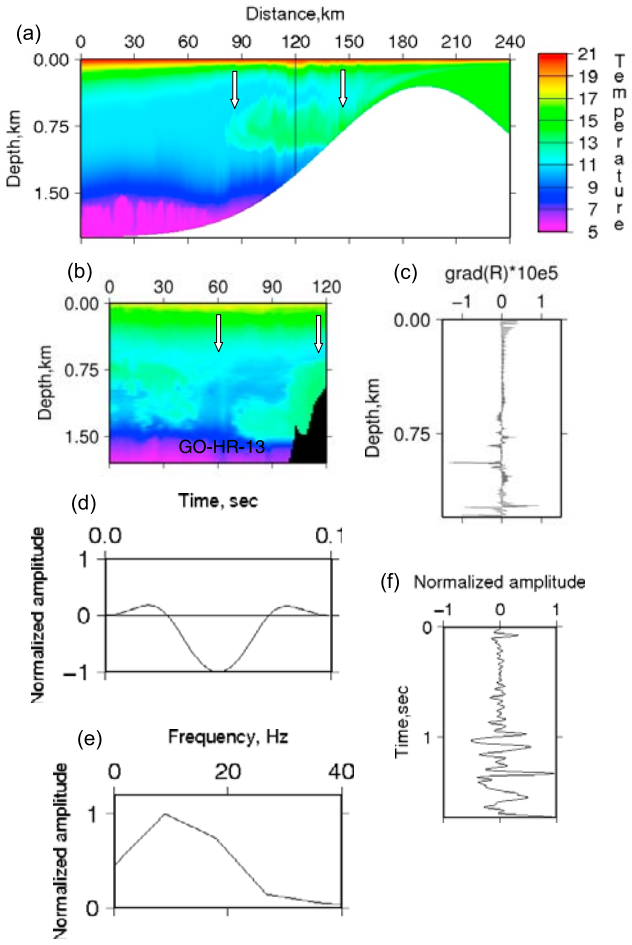

Figure 3. (a) Oceanographic model "Gravity flow over sill". Temperature field for the time screen used later for simulation of the "static" water dataset. The sampling is 160 m in horizontal direction and 2 m in vertical, the vertical line at 120 km shows the position of CTD profiles used to obtain reflectivity profile. (b) Temperature section co-located with GO-HR-13 (location for GO-HR-13 is given in the Figure 1a). A two-layer system clearly seen, which is reproduced well in Figure 3a. White arrows show what the length of the plume. (c) Graded reflection coefficient of CTD profile at 120 km (across plume) down to ocean bottom. Small steps in reflectivity are numerical simulation noise. The gradation is chosen so as to accentuate steps in reflection coefficient. Profile location is shown with vertical line in Figure 3a. (d) Zero-phase Ricker wavelet with peak frequency 10 Hz. (e) Spectrum of the Ricker wavelet. (f) Convolution of the Ricker wavelet (Figure 3d) with reflectivity shown in Figure 3c. Note that only large steps in reflectivity are resolved.

the requirements of seismic modelling with that of the dynamic oceanographic dataset with the sufficient sampling is still numerically challenging.

[18] Figure 3c shows the gradient of the reflection coefficient $R = (Z_j - Z_{j-1})/(Z_j + Z_{j-1})$, where $Z_j = c_j \cdot \rho_j$ is the acoustic impedance [*Ruddick et al.*, 2009] (c_j and ρ_j are sound-speed and density in a layer j, respectively). Small steps in the profile are numerical simulation noise. For a Ricker wavelet with peak frequency of 10 Hz (Figures 3d and 3e) (wavelength of 150 m) we have a resolution limit of $\lambda/4$ = 37.5 m (Rayleigh criterion). We then convolve the reflectivity (Figure 3c) with this zero phase Ricker wavelet to predict the seismic response. Figure 3f shows the result of the convolution. All small scale changes in the reflectivity profile disappear, leaving only the large steps visible.

4. Simulations Above the Oceanographic Dataset

[19] The oceanographic model covers a 30 hours interval and produces a snapshot of the water structure (temperature, salinity) derived every 15 minutes on a 2D section 250 km wide by 2 km deep with a horizontal and vertical grid size of 160 × 2 m respectively. However, for the seismic simulation, based on the acquisition used during the GO experiment, we should use 40 m shot spacing with a 20 s shot interval, corresponding to a ship speed over the ground of close to 4 knots. Hence to model the seismic response, we require a snapshot every 20 seconds and, to avoid serious spatial aliasing problems, a horizontal and vertical grid size of 20 m × 4 m respectively.

[20] We approached this interpolation issue in four steps:

[21] 1. Windowing the original model data in time and space centred on time and location of seismic shots to be modelled.

[22] 2. Cubic spline interpolation between original 15 min screens to give a time slice every 20 sec.

[23] 3. Cubic spline interpolation in the horizontal spatial domain to resample from 160 m to 20 m and from 2 m to 4 m in vertical direction.

[24] 4. Finally we converted the data to a format compatible with a phase-screen modelling program to compute the seismic shot response.

[25] The seismic simulation parameters were: source function – zero phase Ricker wavelet with peak frequency 10 Hz; offset 4.5 km; shot spacing 20 sec (40 m); receiver spacing – 20 m, tow depth of 5 m. The cubic spline interpolation was adopted in order to avoid any discontinuities when calculating the velocity/density field. The synthetic seismic reflection data modelled using a finite-difference acoustic code with the model defined by acoustic sound-speed and density.

5. Results

[26] We repeated the simulations as for the simple cosine wave model. Figure 4a represents the synthetic data set for "static water". You can see here an actual extent of the slope of topography and the mixing process. Figure 4b shows the gradient of the acoustic impedance for the same time snapshot used for Figure 4a. There is a perfect agreement between brightest reflectors in seismic section and contrasts in gradient impedance map.

[27] Figures 4c and 4d represent "forward" and "backward" synthetic datasets, respectively. As expected the apparent lengths of the events are distorted. When vessel is moving in the same direction as the outflow water we are capturing longer reflector images whereas when the vessel is moving against the outflow water the seismic section gives an image which is seemingly shorter than the real reflector. The spectral content inferred from digitized reflectors for all three stacked data shows different spectral slopes

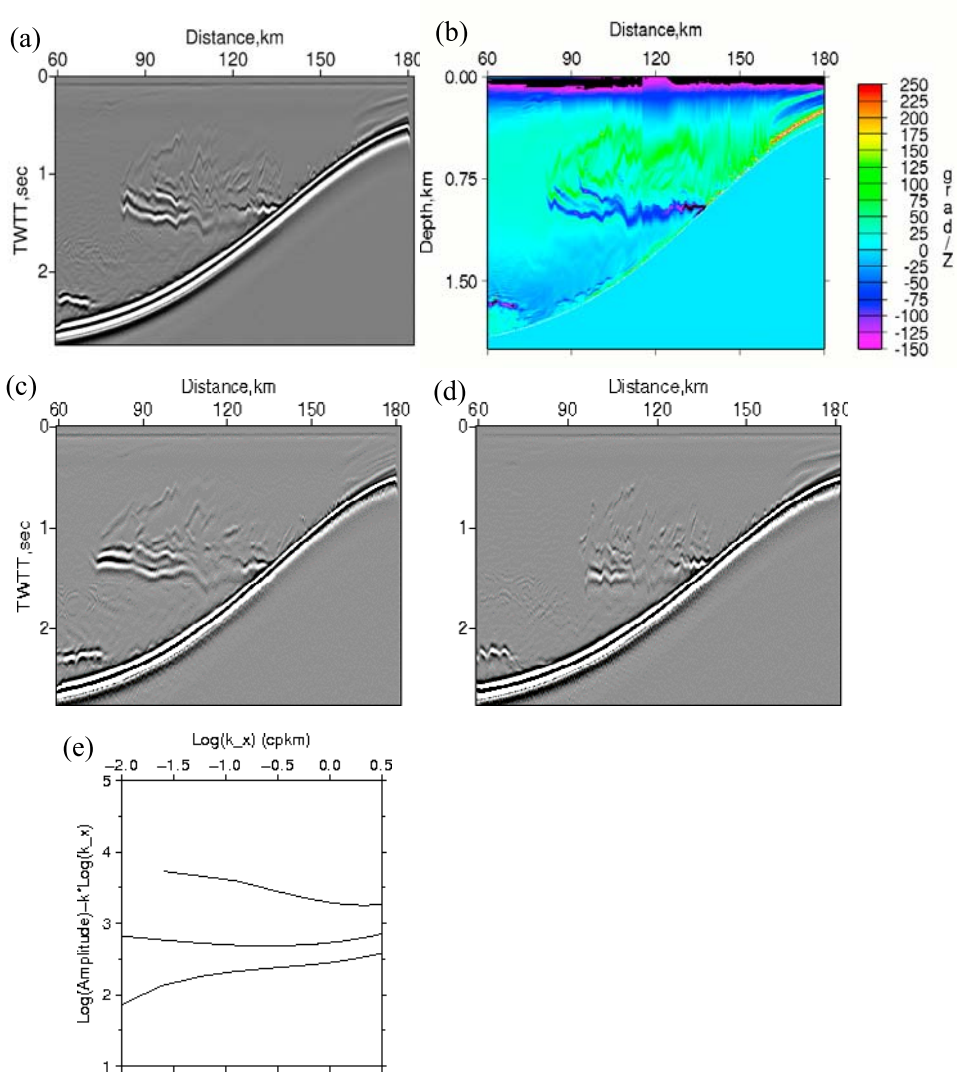

Figure 4. Stack of 2D synthetics for the seismic surveys over the 3 targets, and gradient of impedance for the "static" model: (a) "Static" simulations, where the vessel is moving, but the water is static. (b) Impedance gradient for the time screen used in the model. Note there is a good agreement both of form and location between extrema impedance gradient and brightest reflectors in the stack section. (c) "Forward" simulations (vessel is moving in the same direction as the outflow water). (d) "Backward" simulations (vessel is moving against the outflow water). (e) A comparison of spectral slopes ("best fit" curve) derived by digitizing reflectors in the stack sections in reduced wavenumber space (this domain is used in order to emphasize differences in spectral slope depending on the relative movement of the internal waves and seismic acquisition vessel). The curve close to horizontal is the "true" spectral slope for the "static" model. The curve below is the "forward" model, which gives a flatter spectral slope than the actual "static" case. The top curve is the best fit curve for the spectrum derived from the "backward" dataset, which shows a greater slope than the "static" case.

[*Holbrook and Fer*, 2005] (Figure 4e). We present here the least squares best fit curves for spectra calculated for the same horizons on the stacks shown on Figures 4a, 4c, and 4d. These are shown in the reduced wavenumber domain where the spectral slope of the "true" event (i.e., that obtained above the "static" model) would give a horizontal line. For "contraflow" water the spectral slope is greater than that obtained using correct geometry ($k_{backward} - k_{true} = -0.41$), as estimated for best fit curve. Likewise for a vessel moving with the outflow water the spectrum is flatter than it would be for the real event ($k_{forward} - k_{true} = 0.51$). One difference between this model, and the cosine model is that here we had not introduced seismic reflectors, but smoothed changes of water characteristics. Still the observed effect of the movement on the spectral slope is significant.

6. Discussions and Conclusions

[28] The lateral resolution of *in situ* oceanographic measurements is important, not only in the study of thermohaline fine-structure but also in mesoscale synoptic studies. MCS successfully fills the gap with its ability to image events for tens of kilometers with resolution of a few meters. The simulations presented here aim to illustrate that understanding moving water effect is crucial for any seismic ocean-

ography experiment. Both models – Figures 2 and 4 – show that when the water moves with velocity that is significant to velocity of seismic acquisition vessel we record different images of the boundaries in water. However to the date there are only limited methods estimate water movement during an MCS survey either using a ship born ADCP (acoustic Doppler current profilers) but these only sample the upper 500 m, or XCP (expendable current profiler) [*Nakamura et al.*, 2006]. An alternative is the use an LADCP (lowered acoustic Doppler current profilers) but this requires a second vessel and there are issues of how close in time and location the measurement can be made to the MCS survey. These measurements can provide information on the movement of water masses but do not provide information on the movement of internal waves along the boundaries.

[29] The approach introduced by *Holbrook and Fer* [2005] and further developed by *Krahmann et al.* [2008] deriving spectra from digitized reflection horizons should be applied with care as these are probably distorted by the relative movement of water and seismic acquisition vessel.

[30] *Garrett and Munk* [1972, 1979] present support for the -2 slope on wavenumber spectra related to internal waves. They also note that the spectrum will be modified if there is current past the moored sensor. Here we demonstrate that we compound this problem by also towing the sensor. The apparent change in slope may be critical in the interpretation: a slope of -2 is indicative of internal waves, whereas a slope of -1.67 is characteristic of turbulent mixing. It is therefore necessary to estimate the relative movement of the ship and water target in order to properly quantify the uncertainty in measurements based on MCS data. As the apparent wavelength will change the slope of wavelength spectra estimated from seismic data which may lead to mistaken assumptions about mixing and turbulence in the area where the seismic dataset collected. By correcting the geometry of the relative movement of ship and water the correct wavelength can be recovered, but it raises the question of how to determine an unknown movement [*Klaeschen et al.*, 2009]. If the movement is known, then one may to address this problem by reassigning the geometry to the Legendrian reference frame of the moving water.

[31] **Acknowledgments.** The work was funded by the EU GO-project (NEST-2003 FP6-15603). The authors would like to acknowledge all GO participants for valuable discussions. Seismic sections were produced using Landmark Promax and Seismic Unix software and visualization was carried out using GMT. R.W.Hobbs was a NERC Advanced Research Fellow (NER/J/S/2002/00745).

References

Ambar, I., N. Serra, M. J. Brogueira, G. Cabecadas, F. Abrantes, P. Freitas, P. Goncalves, and N. Gonzalez (2002), Physical, chemical and sedimentological aspects of the Mediterranean Outflow off Iberia, *Deep Sea Res., Part II*, *49*, 4163–4177, doi:10.1016/S0967-0645(02)00148-0.

Armi, L., and D. Farmer (1988), The flow of Mediterranean water through the Strait of Gibraltar, *Prog. Oceanogr.*, *21*, 1, doi:10.1016/0079-6611(88)90055-9.

Garrett, C., and W. Munk (1972), Space-time scales of internal waves, *Geophys. Fluid Dyn.*, *3*, 225–264, doi:10.1080/03091927208236082.

Garrett, C., and W. Munk (1979), Internal waves in the ocean, *Annu. Rev. Fluid Mech.*, *11*, 339–369, doi:10.1146/annurev.fl.11.010179.002011.

Haidvogel, D. B., H. G. Arango, K. Hedstrom, A. Beckmann, P. Malanotte-Rizzoli, and A. F. Shchepetkin (2000), Model evaluation experiments in the North Atlantic basin: Simulations in nonlinear terrain-following coordinates, *Dyn. Atmos. Oceans*, *32*, 239–281, doi:10.1016/S0377-0265(00)00049-X.

Hobbs, R. W. (2007), GO—Geophysical Oceanography: A new tool to understand the thermal structure and dynamics of oceans, periodic report, 59 pp., Durham Univ, Durham, U. K.

Holbrook, W. S., and I. Fer (2005), Ocean internal wave spectra inferred from seismic reflection transects, *Geophys. Res. Lett.*, *32*, L15604, doi:10.1029/2005GL023733.

Holbrook, W. S., P. Paramo, S. Pearce, and R. W. Schmitt (2003), Thermohaline fine structure in an oceanographic front from seismic reflection profiling, *Science*, *301*, 821–834, doi:10.1126/science.1085116.

Kelly, K. R., R. W. Ward, S. Treitel, and R. M. Alford (1976), Synthetic seismograms: a finite-difference approach, *Geophysics*, *41*, 2–27, doi:10.1190/1.1440605.

Klaeschen, D., R. W. Hobbs, G. Krahmann, C. Papenberg, and E. Vsemirnova (2009), Estimating movement of reflectors in the water column using seismic oceanography, *Geophys. Res. Lett.*, *36*, L00D03, doi:10.1029/2009GL038973.

Krahmann, G., P. Brandt, D. Klaeschen, and T. Reston (2008), Mid-depth internal wave energy off the Iberian Peninsula estimated from seismic reflection data, *J. Geophys. Res.*, *113*, C12016, doi:10.1029/2007JC004678.

Nakamura, Y., T. Noguchi, T. Tsuji, S. Itoh, H. Niino, and T. Matsuoka (2006), Simultaneous seismic reflection and physical oceanographic observations of ocean fine structure in the Kuroshio extension front, *Geophys. Res. Lett.*, *33*, L23605, doi:10.1029/2006GL027437.

Ruddick, B., H. Song, C. Dong, and L. Pinheiro (2009), Water column seismic images as maps of temperature gradient, *Oceanography*, *22*, 185–198.

Serra, N., I. Ambar, and R. H. Kaese (2005), Observations and numerical modelling of the Mediterranean Outflow splitting and eddy generation, *Deep Sea Res., Part II*, *52*, 383–408, doi:10.1016/j.dsr2.2004.05.025.

Wild, A. J., R. W. Hobbs, and L. Frenje (2000), Modelling complex media: An introduction to the phase-screen method, *Earth Planet. Sci. Lett.*, *120*, 219–225.

R. Hobbs and E. Vsemirnova, Earth Sciences Department, Durham University, Durham DH1 3LE, UK. (ekaterina.vsemirnova@durham.ac.uk)

D. Klaeschen, Leibniz Institute of Marine Sciences at Kiel University (IFM-GEOMAR), Wischhofstr. 1-3, D-24148 Kiel, Germany.

E. Quentel, LDO, UMR 6538, IUEM, Brest University, CNRS, Place Nicolas Copernic, F-29280 Plouzane CEDEX, France.

N. Serra, Institute of Oceanography, Hamburg University, Bundesstr. 53, D-20146 Hamburg, Germany.